Editors' Suggestion | Featured in Physics

Matched Guiding and Controlled Injection in Dark-Current-Free, 10-GeV-Class, Channel-Guided Laser-Plasma Accelerators

A. Picksley,[1,*] J. Stackhouse,[1,2] C. Benedetti,[1] K. Nakamura,[1] H. E. Tsai,[1] R. Li,[1,2] B. Miao,[3] J. E. Shrock,[3] E. Rockafellow,[3] H. M. Milchberg,[3,4] C. B. Schroeder,[1,2] J. van Tilborg,[1] E. Esarey,[1] C. G. R. Geddes,[1] and A. J. Gonsalves[1]

[1]*Lawrence Berkeley National Laboratory, Berkeley, California 94720, USA*
[2]*University of California, Berkeley, California 94720, USA*
[3]*Institute of Research in Electronics and Applied Physics and Department of Physics, University of Maryland, College Park, Maryland 20742, USA*
[4]*Department of Electrical and Computer Engineering, University of Maryland, College Park, Maryland 20742, USA*

(Received 25 July 2024; accepted 18 October 2024; published 18 December 2024)

We measure the high-intensity laser propagation throughout meter-scale, channel-guided laser-plasma accelerators by adjusting the length of the plasma channel on a shot-by-shot basis, showing high-quality guiding of 500 TW laser pulses over 30 cm in a hydrogen plasma of density $n_0 \approx 1 \times 10^{17}$ cm^{-3}. We observed transverse energy transport of higher-order modes in the first ≈12 cm of the plasma channel, followed by quasimatched propagation, and the gradual, dark-current-free depletion of laser energy to the wake. We quantify the laser-to-wake transfer efficiency limitations of currently available petawatt-class lasers and demonstrate via simulation how control over the laser mode can significantly improve beam parameters. Using 21.3 J of laser energy, and triggering localized electron injection, we observed electron bunches with single, quasimonoenergetic peaks up to 9.2 GeV with charge extending beyond 10 GeV.

DOI: 10.1103/PhysRevLett.133.255001

Particle acceleration in plasma waves driven by intense laser pulses [1–3] has attracted significant attention due to the ultrahigh accelerating gradients that can be achieved (hundreds of GV/m). Compact laser-plasma accelerators (LPAs) are attractive for applications such as free-electron lasers [4,5], Thomson sources [6], and colliders [7,8]. Significant progress has been made toward producing high-energy (> 1 GeV) [9–17], high-quality [18–21] electron bunches using LPAs.

Maximizing electron beam energy for a given laser energy requires maintaining laser intensity over tens of centimeters, much longer than the typical Rayleigh length $z_R \sim 1$ cm of focused, petawatt peak power laser systems. Hence, laser pulses must be guided via relativistic self-focusing [22] or using a preformed plasma channel [23,24]. The former requires operating in the bubble regime of the LPA [25,26], at a plasma density n_0 high enough to remain above the critical power for self-focusing. High-energy electrons can be produced, but high pulse energy is required [2]; for example, Aniculaesei *et al.* [17] demonstrated an energy gain of ∼10 GeV using 118 J of laser energy. Preformed plasma channels have transverse density profiles with a minimum on axis such that the refractive index is peaked, much like gradient-index optical fibers. They allow operation of LPAs at lower n_0 where the product of accelerator gradient and length is higher.

Matching the drive laser to the fundamental transverse mode of the plasma channel maximizes the laser-to-wake energy transfer efficiency and enables high-quality beams. For a parabolic channel where $n_e(r) - n_0 \propto r^2$, a low-intensity laser pulse with a Gaussian transverse profile is perfectly matched to the fundamental channel mode and propagates at constant spot size if $w_0 = w_m$, where w_m is the matched spot size, a measure of the steepness of the parabolic profile [2,23]. Applications of 10-GeV-class LPAs require matched propagation of PW-class lasers with $w_m \lesssim 50$ μm at $n_0 \approx 1 \times 10^{17}$ cm^{-3} [7,8].

Capillary-discharge waveguides [27,28] have previously been employed in multi-GeV LPAs [9,13]. While they are approximately parabolic, and can provide per-mille level stability of w_m and n_0 [29], w_m is too large for sufficient confinement at $n_0 \approx 10^{17}$ cm^{-3}. Even with the addition of an auxiliary laser to reduce w_m [30,31], effective guiding was only achieved above optimal n_0, limiting energy gain to 7.8 GeV [14]. This can be overcome using channels formed by hydrodynamic expansion of optical field-ionized (HOFI) plasmas. Steep channels with $20 \lesssim w_m \lesssim 50$ μm and $n_0 \lesssim 10^{17}$ cm^{-3} can be generated [32–38]. Guiding of high-intensity pulses [34,35,37,39–41] and electron acceleration [15,16,42] have been demonstrated, with ∼5 GeV the highest energy to date [15]. In such experiments, guiding is assessed at the end of the accelerator, and propagation of the laser pulse throughout the plasma is inferred from simulations. Laser mode beating and

*Contact author: apicksley@lbl.gov

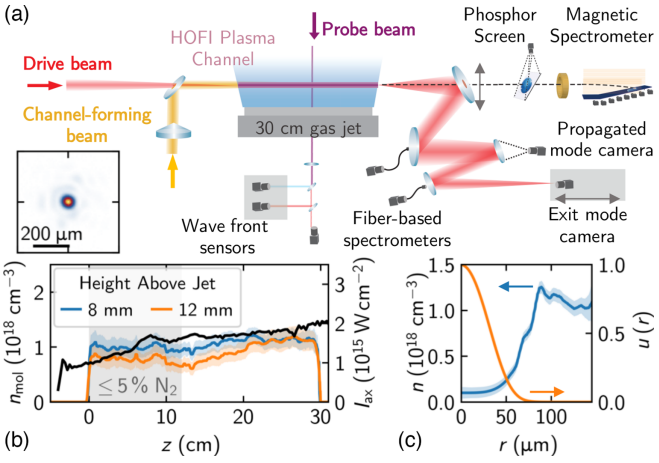

FIG. 1. (a) Schematic of the experimental setup. Inset: measured vacuum mode of the drive laser pulse. (b) Measured molecular density of the gas jet (blue and orange lines) and peak intensity of the channel-forming pulse along the length of the gas (black line). (c) Measured electron and neutral density $n = n_e + n_n$ of the HOFI plasma channel at $\Delta\tau = 6$ ns (blue) and calculated fundamental mode of the measured plasma channel (orange line).

evolution theory [43–46] was recently analyzed via particle-in-cell simulations showing mismatched guiding linked to measured electron spectra [47].

In this Letter, we measure high-intensity, nonlinear laser propagation throughout meter-scale LPAs by adjusting the accelerator length on a shot-by-shot basis, showing high-quality guiding of 500 TW pulses throughout a 30-cm-long hydrogen plasma with $n_0 \approx 1 \times 10^{17}$ cm^{-3}. We show laser pulse coupling into the higher-order channel modes and energy loss through mode filtering, followed by quasi-matched propagation of the fundamental mode, and the gradual, dark-current-free depletion of laser energy to the plasma wave. Then, by triggering electron injection via the localized addition of nitrogen to the plasma, bunches with single, quasimonoenergetic peaks up to 9.2 GeV and charge extending to > 10 GeV are achieved using just (21.3 ± 0.3) J of laser energy. We quantify the laser-to-wake transfer efficiency limitations of currently available PW-class laser systems and demonstrate via simulation how control over the laser mode can result in $\gtrsim$13 GeV bunches for the same channel.

The Ti:sapphire BELLA PW laser [48] produces pulses of FWHM duration ~40 fs at a central wavelength $\lambda_0 = 815$ nm. Recent upgrades allow the amplified laser to be split into two separately compressed beam lines [49] with control over the relative timing, wave front, and focusing geometry. Figure 1(a) shows a schematic of the experimental setup. In the channel-forming beam line, (1.3 ± 0.3) J was focused by an axicon lens and reflected by a mirror with a hole drilled in the center into the gas target [15,34,35,40]. The peak intensity I_{ax} as a function of distance from the entrance of the gas jet z is shown (black line) in Fig. 1(b). The drive pulse was focused to a spot size $w_0 = (53 \pm 1)$ μm at the entrance of the gas target. The energy was varied up to a maximum of $\mathcal{E}_0 = (21.3 \pm 0.3)$ J, corresponding to a peak normalized vector potential $a_0 \approx 2.2$, where $a_0 \approx 0.85\lambda_0\,[\mu\text{m}]\sqrt{I_0[10^{18}\ \text{W cm}^{-2}]}$, with I_0 the peak intensity.

The diagnostics for the drive laser and electron bunches are described in Refs. [14,48]. The input and guided mode of the drive laser could be imaged over ~60 cm; the propagated drive was also imaged at the plane of the third wedge ≈10 m downstream of the channel exit. The optical spectrum was measured using fiber-based spectrometers covering the wavelength range $400 \lesssim \lambda \lesssim 2200$ nm. The energy transmission $T(z) = \mathcal{E}(z)/\mathcal{E}_0$ was retrieved by integrating the counts on the detector at $z \approx 10$ m, and then using the measured optical spectrum to correct for the detector spectral response. The transverse profile of the electron beam was measured by a phosphor screen placed 12 m downstream of the interaction before the beam entered a 2.5-m-long magnetic spectrometer, with a ±1 mrad angular acceptance.

A 30-cm-long gas target was developed [15,50,51], comprising an elongated, converging-diverging nozzle operated with hydrogen, or hydrogen with a ≤ 5% nitrogen dopant. The length could be varied by blocking the flow of gas above the nozzle. Figure 1(b) shows the molecular density as a function of distance along the gas jet [15]. The delay between the channel-forming laser and the drive laser was varied between $\Delta\tau = 5$ ns and $\Delta\tau = 7$ ns, for which w_m remained unchanged within experimental error. The jet was operated 12 mm below the laser axis to avoid blocking the channel-forming laser (which had a radius of ≈12 mm at $z = 0$). For these conditions, two-color interferometry measurements [37,52,53] shown in Fig. 1(c) indicated an axial plasma density $n_0 \approx 1 \times 10^{17}$ cm^{-3} and matched spot size $w_m \approx 37$ μm.

The evolution of key drive laser parameters for two different laser energies, $\mathcal{E}_0 = (6.0 \pm 0.1)$ J ($a_0 \approx 1.3$) and (19.6 ± 0.4) J ($a_0 \approx 2.2$), and $\Delta\tau = 6$ ns is shown in Fig. 2. Only shots for which the transverse position of the focus with respect to the channel entrance $\Delta R < 25$ μm were included, inferred from a nondestructive centroid diagnostic [54]. This condition was satisfied for 71% of shots. Figure 2(a) shows representative transverse fluence profiles of the drive laser for several different channel lengths ≈10 m downstream of the waveguide exit. For $L_{ch} \approx 7$ cm the drive laser mode had transformed from the top-hat-like input mode (that is typical of currently available PW-class systems based on bulk crystal) to near-Gaussian; the super-Gaussian [55] fit order reduced from ≈6 to ≈2. Through $z \approx 12$ cm, the propagated mode exhibited rings outside the central fluence peak. As the channel was lengthened, a single, approximately Gaussian transverse profile was always observed when the drive laser was well aligned to the channel. Figure 2(b) shows the

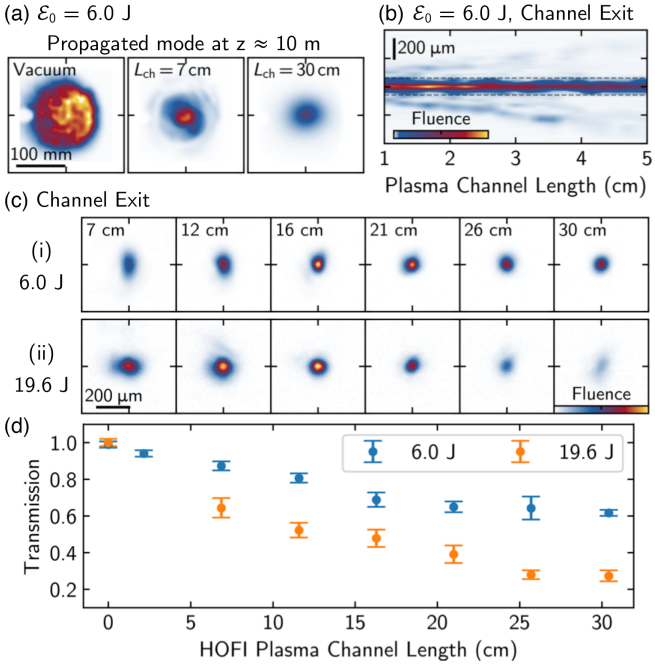

FIG. 2. Evolution of the drive laser in HOFI channels with $n_0 \approx 1 \times 10^{17}$ cm^{-3} and $w_m \approx 37$ μm. (a) Propagated mode $z \approx 10$ m downstream. (b) Lineouts of the exit mode for short channel lengths. The dashed line indicates the measured peak of the neutral density profile. (c) Exit modes for (i) $\mathcal{E}_0 = (6.0 \pm 0.1)$ J and (ii) (19.6 ± 0.4) J. (d) Measured energy transmission averaged over ≈20 shots.

reimaged exit mode, with the channel length varied in steps of 0.2 cm up to $L_{ch} \approx 5$ cm. The dashed line indicates the measured peak of $n(r)$. Figure 2(c) shows reimaged exit mode images for channel lengths ≤ 30 cm. For $z \gtrsim 12$ cm, a well-confined, near-Gaussian drive mode was observed for all channel lengths and for both laser intensities.

Dominant mechanisms behind laser pulse propagation [43,44,47,56] can be understood from these guiding measurements. The channel supports several quasibound modes which we denote as (p, m) referring to the radial and azimuthal mode number, respectively. Their structures are determined by $n_e(r)$. HOFI plasma channels are finite in extent and not radially parabolic; only a finite number of low-order modes can propagate, of which the fundamental (0, 0) [shown in Fig. 1(c), orange line] mode is close to Gaussian. Since the input mode [shown in Fig. 1(a)] was not the fundamental channel mode, energy was coupled into higher-order modes, observed directly from the ring structure in Fig. 2(a) for $L_{ch} \approx 7$ cm. Figure 2(b) shows leakage of higher-order modes out of the bound region at oblique angles over a few centimeters [56]. These modes do not contribute to wakefield generation. After this initial period of mode filtering, which occurred over $z \lesssim 12$ cm, higher-order mode content in the guided mode was severely reduced, evidenced by Fig. 2(c)(i). Remaining higher-order modes slip behind the fundamental due to group velocity dispersion, and eventually become separated longitudinally such that they also do not contribute to wakefield generation [43,44,47,57–61]. The distance over which the (1, 0) and (2, 0) modes separate by 40 fs was calculated to be 21.6 cm, and 9.4 cm, respectively. For $z \gtrsim 12$ cm, the measured exit mode remained approximately Gaussian with measured spot-size oscillation $\lesssim 6\%$, demonstrating approximately matched propagation of the drive in the fundamental mode.

Coupling and propagation losses were evaluated quantitatively. The mode coupling efficiency η of the input drive laser into the measured fundamental mode was calculated as the overlap integral between the two modes. For the measured input spot ($w_0 \approx 53$ μm), $\eta \approx 60\%$. The focus of a perfect near flat-top laser with the same w_0 yields $\eta \approx 72\%$, and for a size of $w_0 \approx 47$ μm, η can be as high as ≈85%. Measured propagation loss [see Fig. 2(d)] is due to transfer of energy to the wake, and the limited angular acceptance of our diagnostics. It was calculated that $> 99\%$, 85%, and 28% of light remaining in the (0, 0), (1, 0), and (2, 0) modes, respectively, was captured inside the diagnostic acceptance. For $\mathcal{E}_0 = (6.0 \pm 0.1)$ J, measured $T(z)$ indicates $(31 \pm 4)\%$ losses in the first 16 cm, consistent with predicted coupling losses. Further losses for $16 \lesssim z \lesssim 30$ cm were $\lesssim 10\%$ indicating mild coupling of remaining energy to the wake. The calculated attenuation through leakage of light remaining in the (1, 0) and (0, 0) modes was small over $16 \lesssim z \lesssim 30$ cm. Since wakefield generation is mainly driven by energy in the (0, 0) mode, and higher-order modes are filtered, control over the channel length directly illustrates how laser-to-wake transfer efficiency is limited in LPAs due to currently available PW-class systems, and can be maximized by careful matching of the laser to the channel.

Driving a wakefield suitable of generating multi-GeV beams required increased laser intensity [2]. Similar behavior of the drive laser evolution for laser energy (19.6 ± 0.4) J is observed in Fig. 2(b)(ii), with the exception of decreased transmission associated with wakefield generation. This was confirmed by laser redshifting shown in Fig. 3(a). Simulations of this case were performed using the code INF&RNO [62,63]. The measured parameters for the laser (energy, and temporal and spatial profiles) and density were used (see Fig. 1). Figure 3(b) shows the calculated optical spectrum. The wavelength at which the spectrum reduces to 5% of the peak, λ_R, is shown in black and matched closely to experiment for all L_{ch}, with continual depletion of energy from the laser to the wake. The calculated average field was $E_z \approx 30$ GV m^{-1} and fraction of energy lost by the laser pulse was 32%. Unlike for $\mathcal{E}_0 = (6.0 \pm 0.1)$ J, at high-intensity $T(z)$ continuously reduced as energy was coupled to the wake [15,35,46,64].

Figure 3(c) (blue line) shows the calculated evolution of the normalized peak intensity $\hat{a}(z)$ for parameters of Fig. 3(b). Oscillations in $\hat{a}(z)$ are due to mode beating

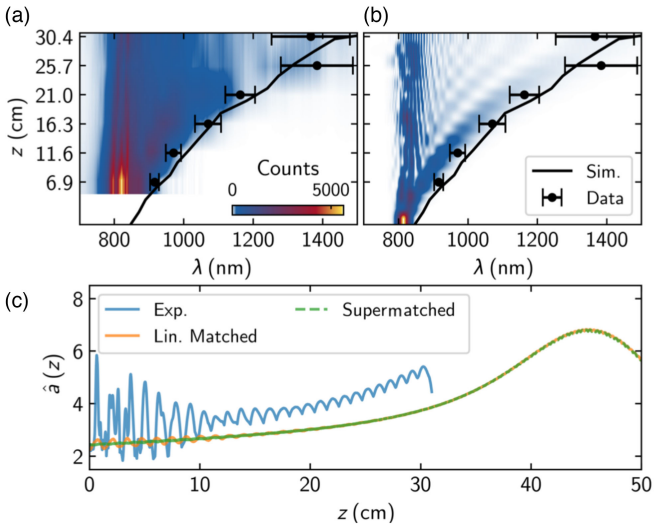

FIG. 3. Measured (a) and simulated (b) optical spectra as a function of propagation distance for $\mathcal{E}_0 = 19.6$ J, $n_0 \approx 1 \times 10^{17}$ cm^{-3}, and $w_m \approx 37$ μm. Measured (averaged over ≈20 shots) and calculated λ_R is overlaid in black. (c) Calculated normalized peak intensity $\hat{a}$ as a function of propagation distance for the experimental input, linearly matched, and supermatched spots.

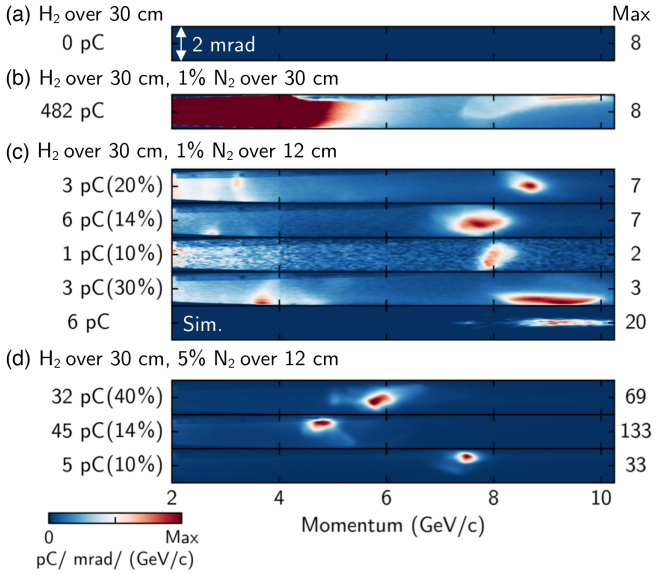

FIG. 4. Example electron beams generated in 30-cm-long HOFI channels with $\mathcal{E}_0 = (21.3 \pm 0.3)$ J. For each row, the charge measured by the spectrometer within the quasimonoenergetic bunch and percent captured by the spectrometer is given. (a) $\Delta\tau = 6$ ns, no nitrogen, (b) $\Delta\tau = 7$ ns, 1% nitrogen, $L_{dop} \approx 30$ cm, (c) $\Delta\tau = 5$ ns, 1% nitrogen, $L_{dop} \approx 12$ cm, (d) $\Delta\tau = 6$ ns, 5% nitrogen, $L_{dop} \approx 12$ cm.

and cause periodic changes in the longitudinal and transverse structure of the wakefield [43,45–47]. Changes in the longitudinal structure result from relativistic effects (i.e., the dependence of the plasma wavelength on the laser strength), while changes in the transverse structure result from laser mode evolution (i.e., the shape of the laser mode varies because of mode beating, and this affects the transverse component of the ponderomotive force). The latter can result in a wakefield unsuitable for the transport of electron beams if, for instance, the laser mode acquires a sufficiently deep minimum on axis. Mode filtering and subsequent mode dispersion reduce the visibility of oscillations for $z \gtrsim 12$ cm, consistent with the diminishing ring structures in Fig. 2(a). Low oscillations caused by beating between the (0, 0) and (1, 0) modes are present as the laser self-steepens and redshifts.

No electron beams were generated for the experiments presented above [see Fig. 4(a)], demonstrating that pulses can be well guided for densities below the self-trapping threshold at intensities sufficient to generate high-amplitude plasma waves. Electron beams were generated by introducing a nitrogen dopant to the gas jet [65–67]. A 1% dopant extending throughout the jet triggered injection at several points and resulted in electron bunch spectra with a broad distribution. Electrons injected after short propagation distance experience the wake over a longer distance and reach higher energies, while electrons injected later in the channel experience less energy gain. An example bunch with conditions similar to Fig. 2 (but with $\Delta\tau = 7$ ns) is shown in Fig. 4(b). A peak in the tail of the distribution was observed at ∼9.4 GeV with charge extending ≳10 GeV.

To study the acceleration of single, quasimonoenergetic bunches, we restricted the dopant region $0 \leq z \lesssim L_{dop}$ within the gas jet [47,68,69]. For $L_{dop} \approx 6$ cm, high-energy electrons were not observed. Figure 4(c) shows generated beams for $L_{dop} \approx 12$ cm, $\Delta\tau = 5$ ns, and $\mathcal{E}_0 = (21.3 \pm 0.3)$ J. Singly peaked electron bunches were observed, indicating injection in the region $6 \lesssim z \lesssim 12$ cm. The mean energy and FWHM spread for the examples in Fig. 4(c) were 8.67 ± 0.48, 7.70 ± 0.88, 7.96 ± 0.44, and 9.15 ± 1.80 GeV. Shot-to-shot stability was dominated by transverse offset of the laser focus at the channel entrance, and by variations of ≳20% in the pulse duration. Because of pointing variations and limited acceptance of the spectrometer, not all of the charge recorded by the phosphor screen was captured by the magnetic spectrometer. For each example, the measured charge within the quasimonoenergetic bunch and percentage of charge captured is shown. The bottom panel in Fig. 4(c) shows results from INF&RNO simulations with the same conditions. The simulation confirmed ionization of nitrogen occurred throughout the dopant region, $z \leq 12$ cm; however, changes in the wake, noted in Fig. 3(a), prevented the trapping of electrons with a significant charge for $z \lesssim 8.6$ cm [16,47]. A portion of the electrons ionized within $8.6 \lesssim z \lesssim 12$ cm were accelerated to 9.3 GeV (FWHM energy spread 1.3 GeV, bunch charge 6 pC).

Optimizing wake-to-bunch energy transfer requires beam loading using a tailored current profile [2,70]. For current profiles providing strong beam loading, the overall

acceleration gradient is reduced. This was demonstrated by increasing the dopant concentration to 5% [see Fig. 4(d)]. The estimated total charge increased by a factor of $\gtrsim 3$, but resulted in a maximum bunch energy of 7.44 GeV (0.25 GeV FWHM energy spread).

Future, high repetition-rate laser systems (e.g., based on fiber lasers [71]) allow for precise control over the transverse laser modes, in contrast to bulk-crystal lasers. For the same laser energy and channel, although with the pulse length optimized for electron beam trapping ($\approx$70 fs) [67], the orange curve in Fig. 3(c) shows the intensity evolution for a linearly matched input mode. Mode beating was greatly reduced, but not eliminated because at these intensities the plasma refractive index itself is modified, slice by slice along the pulse, by relativistic self-focusing and ponderomotive self-channeling [23,45,72]. This simulation produced a 13.0 GeV, 65 pC electron bunch, trapped in the region $z \lesssim 4$ cm, after $z \approx 50$ cm, and the fraction of energy transferred to the wake was 46%. This was compared to the green curve of Fig. 3(c) where the transverse laser mode of each longitudinal slice of the pulse was varied so that it remained matched to the ponderomotively perturbed channel (supermatching) [46]. Mode beating and oscillations in $\hat{a}(z)$ were completely eliminated. The simulated electron bunch was 13.1 GeV, 102 pC after a $z \approx 50$ cm. This demonstrates that control over the laser mode maximizes coupling to the fundamental channel mode, and minimizes the distance over which the wake is unsuitable for electron beam transport. The marginal difference in energy gain between a laser pulse initiated with a supermatched or a linearly matched input mode is encouraging, since it could mitigate the necessity for supermatching. Tailoring of the plasma channel at the entrance of the plasma channel [16,40,73,74] to filter p, $m > 0$ modes more rapidly could also reduce the mode-beating distance.

In conclusion, unprecedented insight into the mechanisms of laser propagation in meter-scale LPAs has been gained through varying the accelerator length on a shot-by-shot basis. We observed laser coupling into high-order channel modes and their energy loss through mode filtering, followed by quasimatched propagation of the fundamental mode, and nonlinear depletion of laser energy to the wake. We quantified the reduction in laser-to-wake efficiency and electron energy gain caused by the laser mode of currently available PW-class lasers, and showed how control over the mode can result in a significant increase of the bunch energy and charge for the same channel. Matched guiding at $n_0 \approx 10^{17}$ cm^{-3} suppressed electron self-trapping throughout the accelerator. With a nitrogen dopant, electron beams were generated with single, quasimonoenergetic peaks up to 9.2 GeV using 21.3 J of laser energy. Previous demonstrations of acceleration to $\sim$7.8 GeV using the same laser system required 31 J and produced electron spectra containing several lower-energy peaks [14]. This Letter opens the door for advanced injection techniques to trap ultralow emittance bunches [75] using plasma structures well suited to repetition rates exceeding 1 kHz [32,76], meeting requirements for future compact accelerators.

Acknowledgments—This work was supported by the Director, Office of Science, Office of High Energy Physics, of the U.S. Department of Energy under Contract No. DE-AC02-05CH11231, the Defense Advanced Research Projects Agency, and used the facilities at the National Energy Research Scientific Computing Center (NERSC). E. R. is supported by NSF Graduate Research Fellowship (DGE 1840340). We greatly acknowledge technical support from Zac Eisentraut, Mark Kirkpatrick, Federico Mazzini, Nathan Ybarrolaza, Derrick McGrew, Teo Maldonado Mancuso, Art Magana, and Joe Riley. The authors would like to thank Nathan Cook, Jens Osterhoff, Davide Terzani, Remi Lehe, Jared De Chant, Liona Fan-Chiang, Lieselotte Obst-Huebl, Marlene Turner, and Aodhan McIlvenny for useful discussions. We thank Samantha Trieu and Chetanya Jain for design support in Fig. 1.

[1] T. Tajima and J. M. Dawson, Laser electron accelerator, Phys. Rev. Lett. **43**, 267 (1979).
[2] E. Esarey, C. B. Schroeder, and W. P. Leemans, Physics of laser-driven plasma-based electron accelerators, Rev. Mod. Phys. **81**, 1229 (2009).
[3] S. M. Hooker, Developments in laser-driven plasma accelerators, Nat. Photonics **7**, 775 (2013).
[4] W. Wang *et al.*, Free-electron lasing at 27 nanometres based on a laser wakefield accelerator, Nature (London) **595**, 516 (2021).
[5] M. Labat *et al.*, Seeded free-electron laser driven by a compact laser plasma accelerator, Nat. Photonics **17**, 150 (2023).
[6] N. D. Powers, I. Ghebregziabher, G. Golovin, C. Liu, S. Chen, S. Banerjee, J. Zhang, and D. P. Umstadter, Quasi-monoenergetic and tunable x-rays from a laser-driven Compton light source, Nat. Publ. Group **8**, 28 (2013).
[7] C. B. Schroeder, E. Esarey, C. G. R. Geddes, C. Benedetti, and W. P. Leemans, Physics considerations for laser-plasma linear colliders, Phys. Rev. ST Accel. Beams. **13**, 101301 (2010).
[8] C. Schroeder, F. Albert, C. Benedetti, J. Bromage, D. Bruhwiler, S. Bulanov, E. Campbell, N. Cook, B. Cros, M. Downer *et al.*, Linear colliders based on laser-plasma accelerators, J. Instrum. **18**, T06001 (2023).
[9] W. P. Leemans, B. Nagler, A. J. Gonsalves, C. Tóth, K. Nakamura, C. G. R. Geddes, E. Esarey, C. B. Schroeder, and S. M. Hooker, GeV electron beams from a centimetre-scale accelerator, Nat. Phys. **2**, 696 (2006).
[10] C. E. Clayton, J. Ralph, F. Albert, R. A. Fonseca, S. H. Glenzer, C. Joshi, W. Lu, K. A. Marsh, S. F. Martins, W. B. Mori, A. Pak, F. S. Tsung, B. B. Pollock, J. S. Ross, L. O. Silva, and D. H. Froula, Self-guided laser wakefield

acceleration beyond 1 GeV using ionization-induced injection, Phys. Rev. Lett. **105**, 105003 (2010).
[11] H. Lu, M. Liu, W. Wang, C. Wang, J. Liu, A. Deng, J. Xu, C. Xia, W. Li, H. Zhang *et al.*, Laser wakefield acceleration of electron beams beyond 1 GeV from an ablative capillary discharge waveguide, Appl. Phys. Lett. **99**, 091502 (2011).
[12] X. Wang *et al.*, Quasi-monoenergetic laser-plasma acceleration of electrons to 2 GeV, Nat. Commun. **4**, 1988 (2013).
[13] W. P. Leemans, A. J. Gonsalves, H. S. Mao, K. Nakamura, C. Benedetti, C. B. Schroeder, C. Toth, J. Daniels, D. E. Mittelberger, S. S. Bulanov, J. L. Vay, C. G. R. Geddes, and E. Esarey, Multi-Gev electron beams from capillary-discharge-guided subpetawatt laser pulses in the self-trapping regime, Phys. Rev. Lett. **113**, 245002 (2014).
[14] A. J. Gonsalves *et al.*, Petawatt laser guiding and electron beam acceleration to 8 GeV in a laser-heated capillary discharge waveguide, Phys. Rev. Lett. **122**, 084801 (2019).
[15] B. Miao, J. E. Shrock, L. Feder, R. C. Hollinger, J. Morrison, R. Nedbailo, A. Picksley, H. Song, S. Wang, J. J. Rocca, and H. M. Milchberg, Multi-GeV electron bunches from an all-optical laser wakefield accelerator, Phys. Rev. X **12**, 031038 (2022).
[16] A. Picksley, J. Chappell, E. Archer, N. Bourgeois, J. Cowley, D. R. Emerson, L. Feder, X. J. Gu, O. Jakobsson, A. J. Ross, W. Wang, R. Walczak, and S. M. Hooker, All-optical GeV electron bunch generation in a laser-plasma accelerator via truncated-channel injection, Phys. Rev. Lett. **131**, 245001 (2023).
[17] C. Aniculaesei, T. Ha, S. Yoffe, L. Labun, S. Milton, E. McCary, M. M. Spinks, H. J. Quevedo, O. Z. Labun, R. Sain *et al.*, The acceleration of a high-charge electron bunch to 10 GeV in a 10-cm nanoparticle-assisted wakefield accelerator, Matter Radiat. Extremes **9**, 014001 (2024).
[18] J. Faure, C. Rechatin, A. Norlin, A. Lifschitz, Y. Glinec, and V. Malka, Controlled injection and acceleration of electrons in plasma wakefields by colliding laser pulses, Nature (London) **444**, 737 (2006).
[19] O. Lundh, J. Lim, C. Rechatin, L. Ammoura, A. Ben-Ismaïl, X. Davoine, G. Gallot, J. P. Goddet, E. Lefebvre, V. Malka, and J. Faure, Few femtosecond, few kiloampere electron bunch produced by a laser-plasma accelerator, Nat. Phys. **7**, 219 (2011).
[20] G. R. Plateau, C. G. R. Geddes, D. B. Thorn, M. Chen, C. Benedetti, E. Esarey, A. J. Gonsalves, N. H. Matlis, K. Nakamura, C. B. Schroeder, S. Shiraishi, T. Sokollik, J. van Tilborg, C. Toth, S. Trotsenko, T. S. Kim, M. Battaglia, T. Stöhlker, and W. P. Leemans, Low-emittance electron bunches from a laser-plasma accelerator measured using single-shot x-ray spectroscopy, Phys. Rev. Lett. **109**, 064802 (2012).
[21] W. T. Wang, W. T. Li, J. S. Liu, Z. J. Zhang, R. Qi, C. H. Yu, J. Q. Liu, M. Fang, Z. Y. Qin, C. Wang, Y. Xu, F. X. Wu, Y. X. Leng, R. X. Li, and Z. Z. Xu, High-brightness high-energy electron beams from a laser wakefield accelerator via energy chirp control, Phys. Rev. Lett. **117**, 124801 (2016).
[22] P. Sprangle, E. Esarey, and A. Ting, Nonlinear theory of intense laser-plasma interactions, Phys. Rev. Lett. **64**, 2011 (1990).
[23] P. Sprangle and E. Esarey, Interaction of ultrahigh laser fields with beams and plasmas, Phys. Fluids B **4**, 2241 (1992).
[24] C. G. Durfee and H. M. Milchberg, Light pipe for high intensity laser pulses, Phys. Rev. Lett. **71**, 2409 (1993).
[25] A. Pukhov and J. Meyer-ter Vehn, Laser wake field acceleration: The highly non-linear broken-wave regime, Appl. Phys. B **74**, 355 (2002).
[26] W. Lu, C. Huang, M. Zhou, W. B. Mori, and T. Katsouleas, Nonlinear theory for relativistic plasma wakefields in the blowout regime, Phys. Rev. Lett. **96**, 165002 (2006).
[27] A. Butler, D. J. Spence, and S. M. Hooker, Guiding of high-intensity laser pulses with a hydrogen-filled capillary discharge waveguide, Phys. Rev. Lett. **89**, 185003 (2002).
[28] D. J. Spence, A. Butler, and S. M. Hooker, Gas-filled capillary discharge waveguides, J. Opt. Soc. Am. B **20**, 138 (2003).
[29] M. Turner, A. J. Gonsalves, S. S. Bulanov, C. Benedetti, N. A. Bobrova, V. A. Gasilov, P. V. Sasorov, G. Korn, K. Nakamura, J. van Tilborg *et al.*, Radial density profile and stability of capillary discharge plasma waveguides of lengths up to 40 cm, High Power Laser Sci. Eng. **9** (2021).
[30] N. A. Bobrova, P. V. Sasorov, C. Benedetti, S. S. Bulanov, C. G. R. Geddes, C. B. Schroeder, E. Esarey, and W. P. Leemans, Laser-heater assisted plasma channel formation in capillary discharge waveguides, Phys. Plasmas **20**, 020703 (2013).
[31] C. Pieronek, A. Gonsalves, C. Benedetti, S. Bulanov, J. Van Tilborg, J. Bin, K. Swanson, J. Daniels, G. Bagdasarov, N. Bobrova *et al.*, Laser-heated capillary discharge waveguides as tunable structures for laser-plasma acceleration, Phys. Plasmas **27**, 093101 (2020).
[32] R. J. Shalloo, C. Arran, L. Corner, J. Holloway, J. Jonnerby, R. Walczak, H. M. Milchberg, and S. M. Hooker, Hydrodynamic optical-field-ionized plasma channels, Phys. Rev. E **97**, 053203 (2018).
[33] R. Shalloo, Hydrodynamic optical-field-ionized plasma waveguides for laser plasma accelerators, Ph.D. thesis, University of Oxford, 2018.
[34] R. J. Shalloo, C. Arran, A. Picksley, A. von Boetticher, L. Corner, J. Holloway, G. Hine, J. Jonnerby, H. M. Milchberg, C. Thornton, R. Walczak, and S. M. Hooker, Low-density hydrodynamic optical-field-ionized plasma channels generated with an axicon lens, Phys. Rev. Accel. Beams **22**, 041302 (2019).
[35] A. Picksley, A. Alejo, R. J. Shalloo, C. Arran, A. von Boetticher, L. Corner, J. A. Holloway, J. Jonnerby, O. Jakobsson, C. Thornton, R. Walczak, and S. M. Hooker, Meter-scale, conditioned hydrodynamic optical-field-ionized plasma channels, Phys. Rev. E **102**, 053201 (2020).
[36] B. Miao, L. Feder, J. E. Shrock, A. Goffin, and H. M. Milchberg, Optical guiding in meter-scale plasma waveguides, Phys. Rev. Lett. **125**, 074801 (2020).
[37] L. Feder, B. Miao, J. E. Shrock, A. Goffin, and H. M. Milchberg, Self-waveguiding of relativistic laser pulses in neutral gas channel, Phys. Rev. Res. **2**, 043173 (2020).
[38] S. M. Mewes, G. J. Boyle, A. F. Pousa, R. J. Shalloo, J. Osterhoff, C. Arran, L. Corner, R. Walczak, S. M. Hooker, and M. Thévenet, Demonstration of tunability of HOFI

waveguides via start-to-end simulations, Phys. Rev. Res. **5**, 033112 (2023).
[39] S. Smartsev, C. Caizergues, K. Oubrerie, J. Gautier, J.-P. Goddet, A. Tafzi, K. T. Phuoc, V. Malka, and C. Thaury, Axiparabola: A long-focal-depth, high-resolution mirror for broadband high-intensity lasers, Opt. Lett. **44**, 3414 (2019).
[40] A. Picksley, A. Alejo, J. Cowley, N. Bourgeois, L. Corner, L. Feder, J. Holloway, H. Jones, J. Jonnerby, H. M. Milchberg, L. R. Reid, A. J. Ross, R. Walczak, and S. M. Hooker, Guiding of high-intensity laser pulses in 100-mm-long hydrodynamic optical-field-ionized plasma channels, Phys. Rev. Accel. Beams **23**, 081303 (2020).
[41] A. J. Ross, J. Chappell, J. J. van de Wetering, J. Cowley, E. Archer, N. Bourgeois, L. Corner, D. R. Emerson, L. Feder, X. J. Gu, O. Jakobsson, H. Jones, A. Picksley, L. Reid, W. Wang, R. Walczak, and S. M. Hooker, Resonant excitation of plasma waves in a plasma channel, Phys. Rev. Res. **6**, L022001 (2024).
[42] K. Oubrerie, A. Leblanc, O. Kononenko, R. Lahaye, I. A. Andriyash, J. Gautier, J.-P. Goddet, L. Martelli, A. Tafzi, K. Ta Phuoc *et al.*, Controlled acceleration of GeV electron beams in an all-optical plasma waveguide, Light **11**, 1 (2022).
[43] E. Esarey and W. P. Leemans, Nonparaxial propagation of ultrashort laser pulses in plasma channels, Phys. Rev. E **59**, 1082 (1999).
[44] E. Esarey, C. B. Schroeder, B. A. Shadwick, J. S. Wurtele, and W. P. Leemans, Nonlinear theory of nonparaxial laser pulse propagation in plasma channels, Phys. Rev. Lett. **84**, 3081 (2000).
[45] C. Benedetti, C. B. Schroeder, E. Esarey, and W. P. Leemans, Quasi-matched propagation of ultra-short, intense laser pulses in plasma channels, Phys. Plasmas **19**, 053101 (2012).
[46] C. Benedetti, F. Rossi, C. B. Schroeder, E. Esarey, and W. P. Leemans, Pulse evolution and plasma-wave phase velocity in channel-guided laser-plasma accelerators, Phys. Rev. E **92**, 023109 (2015).
[47] J. E. Shrock, E. Rockafellow, B. Miao, M. Le, R. C. Hollinger, S. Wang, A. J. Gonsalves, A. Picksley, J. J. Rocca, and H. M. Milchberg, Guided mode evolution and ionization injection in meter-scale multi-GeV laser wakefield accelerators, Phys. Rev. Lett. **133**, 045002 (2024).
[48] K. Nakamura, H. S. Mao, A. J. Gonsalves, H. Vincenti, D. E. Mittelberger, J. Daniels, A. Magana, C. Toth, and W. P. Leemans, Diagnostics, control and performance parameters for the BELLA high repetition rate petawatt class laser, IEEE J. Quantum Electron. **53**, 1 (2017).
[49] M. Turner, S. Bulanov, C. Benedetti, A. Gonsalves, W. Leemans, K. Nakamura, J. Van Tilborg, C. Schroeder, C. Geddes, and E. Esarey, Strong-field QED experiments using the BELLA PW laser dual beamlines, Eur. Phys. J. D **76**, 205 (2022).
[50] M. Krishnan, K. W. Elliott, C. G. R. Geddes, R. A. van Mourik, W. P. Leemans, H. Murphy, and M. Clover, Electromagnetically driven, fast opening and closing gas jet valve, Phys. Rev. ST Accel. Beams **14**, 033502 (2011).
[51] O. Zhou, H.-E. Tsai, T. M. Ostermayr, L. Fan-Chiang, J. Van Tilborg, C. B. Schroeder, E. Esarey, and C. G. Geddes, Effect of nozzle curvature on supersonic gas jets used in laser–plasma acceleration, Phys. Plasmas **28** (2021).
[52] A. J. Gonsalves, T. P. Rowlands-Rees, B. H. P. Broks, J. J. A. M. Vander Mullen, and S. M. Hooker, Transverse interferometry of a hydrogen-filled capillary discharge waveguide, Phys. Rev. Lett. **98**, 025002 (2007).
[53] G. Point, Y. Brelet, L. Arantchouk, J. Carbonnel, B. Prade, A. Mysyrowicz, and A. Houard, Two-color interferometer for the study of laser filamentation triggered electric discharges in air, Rev. Sci. Instrum. **85**, 123101 (2014).
[54] F. Isono, J. van Tilborg, S. K. Barber, J. Natal, C. Berger, H.-E. Tsai, T. Ostermayr, A. Gonsalves, C. Geddes, and E. Esarey, High-power non-perturbative laser delivery diagnostics at the final focus of 100-TW-class laser pulses, High Power Laser Sci. Eng. **9**, e25 (2021).
[55] A super-Gaussian laser intensity profile is defined as $I = A\exp[-(x/w)^n]$, where n is the order of the fit; $n = 2$ represents a Gaussian and $n \gg 1$ indicates a top-hat profile.
[56] T. R. Clark and H. M. Milchberg, Optical mode structure of the plasma waveguide, Phys. Rev. E **61**, 1954 (2000).
[57] C. B. Schroeder, C. Benedetti, E. Esarey, J. Van Tilborg, and W. P. Leemans, Group velocity and pulse lengthening of mismatched laser pulses in plasma channels, Phys. Plasmas **18**, 083103 (2011).
[58] E. Cormier-Michel, E. Esarey, C. Geddes, C. Schroeder, K. Paul, P. Mullowney, J. Cary, and W. Leemans, Control of focusing fields in laser-plasma accelerators using higher-order modes, Phys. Rev. ST Accel. Beams **14**, 031303 (2011).
[59] J. van Tilborg, J. Daniels, A. J. Gonsalves, C. B. Schroeder, E. Esarey, and W. P. Leemans, Measurement of the laser-pulse group velocity in plasma waveguides, Phys. Rev. E **89**, 063103 (2014).
[60] B. Djordjević, C. Benedetti, C. Schroeder, E. Esarey, and W. Leemans, Control of transverse wakefields via phase-matched laser modes in parabolic plasma channels, Phys. Plasmas **26** (2019).
[61] B. Djordjević, C. Benedetti, C. Schroeder, E. Esarey, and W. Leemans, Filtering higher-order laser modes using leaky plasma channels, Phys. Plasmas **25** (2018).
[62] C. Benedetti, C. Schroeder, E. Esarey, C. Geddes, and W. Leemans, Efficient modeling of laser-plasma accelerators with INF&RNO, AIP Conf. Proc. **1299**, 250 (2010).
[63] C. Benedetti, C. B. Schroeder, C. G. R. Geddes, E. Esarey, and W. P. Leemans, An accurate and efficient laser-envelope solver for the modeling of laser-plasma accelerators, Plasma Phys. Controlled Fusion **60**, 014002 (2017).
[64] B. A. Shadwick, C. B. Schroeder, and E. Esarey, Nonlinear laser energy depletion in laser-plasma accelerators, Phys. Plasmas **16**, 056704 (2009).
[65] A. Pak, K. A. Marsh, S. F. Martins, W. Lu, W. B. Mori, and C. Joshi, Injection and trapping of tunnel-ionized electrons into laser-produced wakes, Phys. Rev. Lett. **104**, 025003 (2010).
[66] C. McGuffey, A. G. R. Thomas, W. Schumaker, T. Matsuoka, V. Chvykov, F. J. Dollar, G. Kalintchenko, V. Yanovsky, A. Maksimchuk, K. Krushelnick, V. Y. Bychenkov, I. V. Glazyrin, and A. V. Karpeev, Ionization induced trapping in a laser wakefield accelerator, Phys. Rev. Lett. **104**, 025004 (2010).

[67] M. Chen, E. Esarey, C. B. Schroeder, C. G. R. Geddes, and W. P. Leemans, Theory of ionization-induced trapping in laser-plasma accelerators, Phys. Plasmas **19**, 033101 (2012).
[68] A. J. Gonsalves *et al.*, Laser-heated capillary discharge plasma waveguides for electron acceleration to 8 GeV, Phys. Plasmas **27**, 053102 (2020).
[69] M. Kirchen, P. Messner, P. Winkler, T. Eichner, H. Thomas, L. Jeppe, M. Schnepp, and A. R. Maier, Optimal beam loading in a laser-plasma accelerator, Phys. Rev. Lett. **126**, 1 (2020).
[70] T. Katsouleas, S. Wilks, J. Dawson, and J. Su, Beam loading efficiency in plasma accelerators, Part. Accel. **22**, 81 (1987), https://inspirehep.net/literature/253298.
[71] C. Jauregui, J. Limpert, and A. Tünnermann, High-power fibre lasers, Nat. Photonics **7**, 861 (2013).
[72] P. Sprangle, E. Esarey, and A. Ting, Nonlinear interaction of intense laser pulses in plasmas, Phys. Rev. A **41**, 4463 (1990).
[73] T. M. Antonsen Jr and P. Mora, Leaky channel stabilization of intense laser pulses in tenuous plasmas, Phys. Rev. Lett. **74**, 4440 (1995).
[74] K. Y. Kim, I. Alekseev, J. Fan, E. Parra, and H. M. Milchberg, Plasma waveguides: Addition of end funnels and generation in clustered gases, AIP Conf. Proc. **647**, 646 (2002).
[75] L. L. Yu, E. Esarey, C. B. Schroeder, J. L. Vay, C. Benedetti, C. G. R. Geddes, M. Chen, and W. P. Leemans, Two-color laser-ionization injection, Phys. Rev. Lett. **112**, 125001 (2014).
[76] A. Alejo, J. Cowley, A. Picksley, R. Walczak, and S. M. Hooker, Demonstration of kilohertz operation of hydrodynamic optical-field-ionized plasma channels, Phys. Rev. Accel. Beams **25**, 011301 (2022).